Optical properties of biaxial nanopatterned gold plasmonic nanowired grid polarizer

Lars Martin Sandvik Aas,[1,*] Morten Kildemo,[1] Christian Martella,[2] Maria Caterina Giordano,[2] Daniele Chiappe,[2] and Francesco Buatier de Mongeot[2]

[1] *Deparment of Physics, The Norwegian University of Science and Technology (NTNU), N-7491 Trondheim, Norway*

[2]*Dipartimento di Fisica, Universita di Genova, and CNISM, Via Dodecaneso, 33, 16146 Genova, Italy*

[*]*lars.martin.aas@gmail.com*

Abstract: Gold nanoparticles deposited on self-organized nano-ripple quartz substrates have been studied by spectroscopic Mueller matrix ellipsometry. The surface was found to have biaxial anisotropic optical properties. For electric field components normal to the ripples the periodic and disconnected nature of the in plane nanowires gives rise to an optical response dominated by the localized plasmon resonance. In the direction parallel to the ripples the gold nanoparticles are aligned closely leading to localized plasmon resonances in the infrared. As Au was deposited at an angle oblique to the surface normal, the gold nanoparticles were formed on the side of the ripples facing the incoming evaporation flux. This makes the gold particles slightly inclined, correspondingly the principal coordinate system of the biaxial dielectric tensor results tilted. The anisotropic plasmonic optical response results in a strong polarizing effect, making it suitable as a plasmonic nanowired grid polarizer.

OCIS codes: (260.2130) Ellipsometry and polarimetry; (160.1190) Anisotropic optical materials; (160.3918) Metamaterials; (160.4236) Nanomaterials; (250.5403) Plasmonics.

References and links

1. F. Wagner, S. Haslbeck, and L. Stievano, "Before striking gold in gold-ruby glass," Nature **407**, 691–692 (2000).
2. P. A. Letnes, I. Simonsen, and D. L. Mills, "Substrate influence on the plasmonic response of clusters of spherical nanoparticles," Phys. Rev. B **83**, 075426 (2011).
3. H. A. Atwater and A. Polman, "Plasmonics for improved photovoltaic devices." Nat. Mater. **9**, 205–213 (2010).
4. D. Smith and D. Schurig, "Electromagnetic Wave Propagation in Media with Indefinite Permittivity and Permeability Tensors," Phys. Rev. Lett. **90**, 077405 (2003).
5. A. Belardini, M. C. Larciprete, M. Centini, E. Fazio, C. Sibilia, M. Bertolotti, A. Toma, D. Chiappe, and F. Buatier de Mongeot, "Tailored second harmonic generation from self-organized metal nano-wires arrays." Opt. Express **17**, 3603–3609 (2009).
6. A. Belardini, M. C. Larciprete, M. Centini, E. Fazio, C. Sibilia, D. Chiappe, C. Martella, A. Toma, M. Giordano, and F. Buatier de Mongeot, "Circular Dichroism in the Optical Second-Harmonic Emission of Curved Gold Metal Nanowires," Phys. Rev. Lett. **107**, 257401 (2011).
7. V. Robbiano, M. Giordano, C. Martella, F. D. Stasio, D. Chiappe, F. B. de Mongeot, and D. Comoretto, "Hybrid Plasmonic–Photonic Nanostructures: Gold Nanocrescents Over Opals," Adv. Opt. Mat. **1**, 389–396 (2013).
8. T. Oates, H. Wormeester, and H. Arwin, "Characterization of plasmonic effects in thin films and metamaterials using spectroscopic ellipsometry," Prog. Surf. Sci. **86**, 328–376 (2011).

#197203 - $15.00 USD Received 13 Sep 2013; revised 18 Nov 2013; accepted 18 Nov 2013; published 9 Dec 2013

9. T. W. H. Oates, A. Keller, S. Facsko, and A. Mücklich, "Aligned Silver Nanoparticles on Rippled Silicon Templates Exhibiting Anisotropic Plasmon Absorption," Plasmonics **2**, 47–50 (2007).
10. T. W. H. Oates, M. Ranjan, S. Facsko, and H. Arwin, "Highly anisotropic effective dielectric functions of silver nanoparticle arrays," Opt. Express **19**, 2014–2028 (2011).
11. S. Camelio, D. Babonneau, D. Lantiat, L. Simonot, and F. Pailloux, "Anisotropic optical properties of silver nanoparticle arrays on rippled dielectric surfaces produced by low-energy ion erosion," Phys. Rev. B. **80**, 1–10 (2009).
12. M. Lončarić, J. Sancho-Parramon, and H. Zorc, "Optical properties of gold island films—a spectroscopic ellipsometry study," Thin Solid Films **519**, 2946–2950 (2011).
13. A. J. de Vries, E. S. Kooij, H. Wormeester, A. Mewe, and B. Poelsema, "Ellipsometric study of percolation in electroless deposited silver films," J. Appl. Phys. **101**, 053703 (2007).
14. E. Hecht, *Optics* (Addison Wesley, 2002).
15. A. Toma, D. Chiappe, D. Massabò, C. Boragno, and F. Buatier de Mongeot, "Self-organized metal nanowire arrays with tunable optical anisotropy," Appl. Phys. Lett. **93**, 163104 (2008).
16. L. Anghinolfi, R. Moroni, L. Mattera, M. Canepa, and F. Bisio, "Flexible Tuning of Shape and Arrangement of Au Nanoparticles in 2-Dimensional Self-Organized Arrays: Morphology and Plasmonic Response," J. Phys. Chem. C **115**, 14036–14043 (2011).
17. A. Toma, D. Chiappe, C. Boragno, and F. Buatier de Mongeot, "Self-organized ion-beam synthesis of nanowires with broadband plasmonic functionality," Phys. Rev. B **81** (2010).
18. L. M. S. Aas, I. S. Nerbø, M. Kildemo, D. Chiappe, C. Martella, and F. Buatier de Mongeot, "Mueller matrix imaging of plasmonic polarizers on nanopatterned surface," Proc. SPIE **8082**, 80822W (2011).
19. A. Toma, F. Buatier de Mongeot, R. Buzio, G. Firpo, S. Bhattacharyya, C. Boragno, and U. Valbusa, "Ion beam erosion of amorphous materials: evolution of surface morphology," Nucl. Instrum. Methods **230**, 551–554 (2005).
20. D. Chiappe, A. Toma, and F. Buatier de Mongeot, "Tailoring resisitivity anisotropy of nanorippled metal films: Electrons surfing on gold waves," Phys. Rev. B **86**, 045414 (2012).
21. R. M. Bradley and J. M. E. Harper, "Theory of ripple topography induced by ion bombardment," J. Vac Sci. Technol. A **6**, 2390–2395 (1988).
22. W. L. Chan and E. Chason, "Making waves: Kinetic processes controlling surface evolution during low energy ion sputtering," J. Appl. Phys. **101**, 121301 (2007).
23. U. Valbusa, C. Boragno, and F. Buatier de Mongeot, "Nanostructuring by ion beam," Mater. Sci. Eng. C **23**, 201–209 (2003).
24. I. Nerbø, S. L. Roy, M. Foldyna, E. Søndergård, and M. Kildemo, "Real-time in situ Mueller matrix ellipsometry of GaSb nanopillars: observation of anisotropic local alignment," Opt. Express **19**, 571–575 (2011).
25. M. Schubert, "Generalized ellipsometry and complex optical systems," Thin Solid Films **313-314**, 323–332 (1998).
26. D. Schmidt, B. Booso, T. Hofmann, E. Schubert, A. Sarangan, and M. Schubert, "Generalized ellipsometry for monoclinic absorbing materials: determination of optical constants of Cr columnar thin films." Opt. Lett. **34**, 992–4 (2009).
27. R. Azzam and N. Bashara, *Ellipsometry and Polarized light* (North-Holland, 1977).
28. P. S. Hauge, R. H. Muller, and C. G. Smith, "Conventions and formulas for using the Mueller-Stokes calculus in ellipsometry," Surf. Sci. **96**, 81–107 (1980).
29. T. Yamaguchi, S. Yoshida, and a. Kinbara, "Optical effect of the substrate on the anomalous absorption of aggregated silver films," Thin Solid Films **21**, 173–187 (1974).
30. T. Yamaguchi, H. Takahashi, and A. Sudoh, "Optical behavior of a metal island film," J. Opt. Soc. Am. **68**, 1039 (1978).
31. J. Spanier and I. Herman, "Use of hybrid phenomenological and statistical effective-medium theories of dielectric functions to model the infrared reflectance of porous SiC films," Phys. Rev. B **61**, 10437–10450 (2000).
32. G. A. Niklasson and C. G. Granqvist, "Optical properties and solar selectivity of coevaporated Co-Al2O3 composite films," J. Appl. Phys. **55**, 3382 (1984).
33. R. Lazzari and I. Simonsen, "GranFilm: a software for calculating thin-layer dielectric properties and Fresnel coefficients," Thin Solid Films **419**, 124–136 (2002).
34. I. Simonsen, R. Lazzari, J. Jupille, and S. Roux, "Numerical modeling of the optical response of supported metallic particles," Phys. Rev. B **61**, 7722–7733 (2000).
35. S. A. Mayer, *Plasmonics, Fundamentals and Applications* (Springer, 2007).
36. D. De Sousa Meneses, G. Gruener, M. Malki, and P. Echegut, "Causal Voigt profile for modeling reflectivity spectra of glasses," J. Non-Cryst. Solids **351**, 124–129 (2005).
37. E. D. Palik, *Handbook of Optical Constants of Solids I* (Academic, 1985).
38. J. Woollam, B. D. Johs, J. N. Herzinger, M. Craig, J. Hilfiker, R. A. Synowicki, and C. L. Bungay, "Overview of variable-angle spectroscopic ellipsometry (VASE): I. Basic theory and typical applications," Proc. SPIE **CR72**, 3–28 (1999).
39. M. Honkanen, V. Kettunen, M. Kuittinen, J. Lautanen, J. Turunen, B. Schnabel, and F. Wyrowski, "Inverse metal-stripe polarizers," Appl. Phys. B. **68**, 81–85 (1999).

#197203 - $15.00 USD Received 13 Sep 2013; revised 18 Nov 2013; accepted 18 Nov 2013; published 9 Dec 2013

40. A. Drauschke, B. Schnabel, and F. Wyrowski, "Comment on the inverse polarization effect in metal-stripe polarizers," J. Opt. A. **3**, 67–71 (2001).
41. S. Lu and R. Chipman, "Interpretation of Mueller matrices based on polar decomposition," J. Opt. Soc. Am. A. **13**, 1106–1113 (1996).

1. Introduction

The optical excitation of collective oscillations of free electrons from noble metal nanoparticles, known as localized surface plasmon resonances, are known to have spectroscopic properties resulting in *e.g.* various color effects. One example is the well known "Lycurgus cup" [1], in which silver nanoparticles distributed in glass provides a different color to it depending if illumination is performed in transmission or in reflection. It is known that nanoparticle size, spacing and substrate, affects the plasmonic resonance frequency [2], and is an effective way to design selective optical properties. A recent wave of interest in plasmonics is motivated by the proven increase in photon absorption and thus in efficiency of photovoltaic devices [3] caused by the strong localization of the electric field and by enhanced scattering from the metal nanoparticles. On the fundamental level the strongly anisotropic plasmonic nanostructures are used to form metamaterials [4] with possible applications to e.g. negative refractive materials in the visible [4] or in non-linear applications [5–7].

The anisotropic optical response of plasmonic nanoparticles and metamaterials can favourably be studied by spectroscopic generalized ellipsometry, as recently reviewed by Oates *et al.* [8]. In particular, several studies of the optical properties of in plane silver nanowires on various substrates have been reported [9–11], where in particular the effective dielectric tensor of silver nanoparticle arrays on a silicon substrate was determined with spectroscopic Mueller Matrix Ellipsometry [10]. Also ellipsometric studies of isotropic and anisotropic silver and gold island films have been reported [12, 13].

In this work, we are exploring the enhanced sensitivity of Mueller matrix spectroscopic ellipsometry from the ultra violet to the near-infrared, combined with azimuthal rotation of the sample around the sample normal, using multiple angles of incidence, in order to determine the complex biaxial properties of a plasmonic layer of gold nanoparticles supported on a nano-patterned quartz substrate. Such nano-patterned plasmonic wires have many similarities to the standard infrared wire grid polarizer [14]. However, due to the localized plasmons, an inverse polarizing effect can be observed in the visible spectral range using polarized transmission spectroscopy at normal incidence [5, 15]. It has been observed that the anisotropic localized surface plasmonic properties change the polarizing properties of the sample from transverse electric (TE) to transverse magnetic (TM) [16], but the details of the dielectric tensor for such a complex plasmonic system based on aligned and partially connected gold nanoparticles have so far not been reported. The development of systematic optical methods to reveal the dielectric function of such gold based nanoplasmonic samples is further of fundamental interest due to the common use of gold nanoparticles in applications of plasmonics and metamaterials.

The samples studied in this paper were prepared by shadow deposition of gold at grazing incidence onto a quartz self-organized nano-ripple surface produced by ion beam sputtering [15], similar to samples in [17, 18].

2. Experimental

The anisotropic gold nanopatterned surfaces were prepared in a two stage process combining self-organized ion beam sputtering (IBS) to produce ripples on the surface of the quartz substrate, and gold deposition by thermal evaporation. IBS is a low cost nano-fabrication process used to pattern a range of materials from metallic to dielectric [19, 20]. A spatial modulation of the surface profile is induced by a combination of an erosive instability induced by the ion

#197203 - $15.00 USD Received 13 Sep 2013; revised 18 Nov 2013; accepted 18 Nov 2013; published 9 Dec 2013

beam and energy relaxation dominated by the thermally activated diffusion and hyperthermal mobility induced by the ion beam [21,22]. Variations of the surface morphology is made possible by changing the irradiation parameters such as ion energy, incidence angle, gas species, and sample temperature [23]. A clean quartz substrate was irradiated by Ar^+ ions in an ultra high vacuum (UHV) system at an incidence angle of 45°. The ions are ejected from a gridded multi aperture source having an energy of 800 eV at a constant flux of 4.0×10^{15} ions/cm^{2}s. The IBS process results in a surface having a well defined ripple pattern, facing the ion beam. An atomic force microscope (AFM) micrograph of such a surface is shown in Fig. 1(a). The ripples have a period of approximately $\Lambda = 70 \pm 5$ nm and an amplitude around 6 nm.

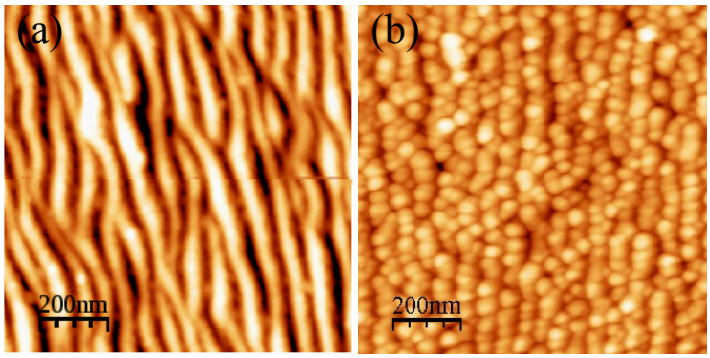

Fig. 1. (a) shows the AFM image of the glass substrate after patterning but prior to deposition of Au. (b) shows the AFM image of the surface after deposition of Au.

Gold was evaporated in the same UHV system onto the surface at a grazing incidence angle (80°), forming nanoparticles on the surface. The spatial distribution of the nanoparticles is locally modulated by the shadowing of the nanoripple ridges, such that more material is deposited onto the facing ridges. The shadowed ridge is then mainly uncovered by Au. During the deposition the distribution of particles are limited in the direction normal to the ripples. In the direction along the ripples, the particles are partially connected, forming in some cases elongated planar nanowires. Figure 1(b) shows an AFM micrograph of the nanopatterned surface.

A schematic of the cross-section of the sample system is shown in Fig. 2, where the coordinate system is aligned with the $x-$axis in the long direction of the nanowires, and the $y-z$ plane rotated by an angle θ so that the $y-$axis is in the plane of the gold nanoparticle-substrate interface. θ is in the following regarded as the tilt angle of the biaxial system. Cross-section electron microscope micrographs were not easily obtained due to the charging of the dielectric substrate. A geometrical model of the nanowires based on the AFM topographies and on the deposited amount of gold, allows to estimate the local height of the Au nanowires ($h = 29.5$ nm) measured along the z-axis and their width ($w = 72$ nm), measured along the y-axis.

For the optical characterization a variable angle multichannel dual rotating compensator Mueller matrix ellipsometer (RC2) from JA Woollam Company was used. The instrument has a collimated 150 W Xe source and operates in the spectral range from 210 nm (5.9 eV) to 1700 nm (0.73 eV), using a combination of silicon and indium gallium arsenide spectrographs having a resolution of 1 nm below 1000 nm and 2.5 nm above. The initial collimated beam has a waist of approximately 3 mm, but in the present work focusing and collection lenses with a focal length of 80 mm were applied, allowing a normal incidence spot size of 150 µm. This spot size allowed us to study a reasonably spatially homogeneous region of the sample [18].

The spectroscopic Mueller matrix was measured for the incidence angles 50° to 75° in steps

#197203 - $15.00 USD Received 13 Sep 2013; revised 18 Nov 2013; accepted 18 Nov 2013; published 9 Dec 2013

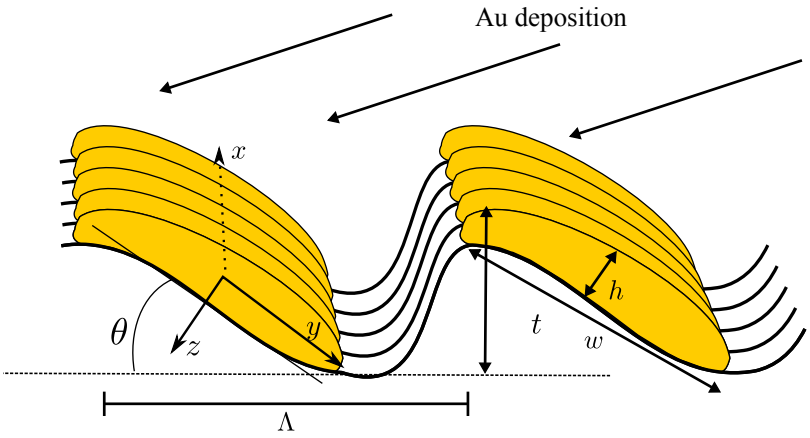

Fig. 2. The gold nanoparticles are preferentially deposited along the ridges of the quartz nanoripples, where nucleation and agglomeration take place. An optical model was based on a biaxial cartesian coordinate system, where the optical axes are indicated to be aligned along the nanowires ($x-$axis), along the slope of the ripples, and normal to the ripple edge. The tilt angle θ is indicated as the local slope. The thickness of the effective layer is h.

of 5°. Full azimuthal rotation of the sample (360°) in steps of 5° was performed for each angle of incidence in order to fully map the anisotropy of the sample. When using focusing optics the sample alignment upon rotation is very sensitive, and was therefore adjusted prior to the measurement of each incidence angle. The same instrument was also used to measure the spectroscopic transmission Mueller matrix of the sample.

3. Theory

With ellipsometry, the polarization nature of light is used to indirectly measure extrinsic and intrinsic properties of *e.g.* thin films, nanostructures or bulk materials [24–26]. In specific, the change of polarization state of monochromatic light upon reflection from a smooth surface can be formulated by the 2×2 complex Jones matrix transforming the incoming polarization state to the reflected by the Fresnel coefficients (r_{pp}, r_{ps}, etc.) by [27]

$$\begin{bmatrix} E_p \\ E_s \end{bmatrix}^{\text{refl}} = \begin{bmatrix} r_{pp} & r_{ps} \\ r_{sp} & r_{ss} \end{bmatrix} \begin{bmatrix} E_p \\ E_s \end{bmatrix}^{\text{inc}} \tag{1}$$

E_p and E_s are orthogonal plane wave electric field components, where E_p is parallel and E_s perpendicular to the incidence plane. In practical applications, in Mueller matrix polarimetry and ellipsometry in particular, the polarization state is commonly described using the four element Stokes vector

$$S = \begin{bmatrix} s_0 \\ s_1 \\ s_2 \\ s_3 \end{bmatrix} = \begin{bmatrix} I_p + I_s \\ I_p - I_s \\ I_{+45^\circ} - I_{-45^\circ} \\ I_R - I_L \end{bmatrix} = \begin{bmatrix} \langle E_{p0}(t)^2 \rangle + \langle E_{s0}(t)^2 \rangle \\ \langle E_{p0}(t)^2 \rangle - \langle E_{s0}(t)^2 \rangle \\ 2\langle E_{p0}(t) E_{s0}(t) \cos\delta(t) \rangle \\ 2\langle E_{p0}(t) E_{s0}(t) \sin\delta(t) \rangle \end{bmatrix}. \tag{2}$$

Where the elements s_0, s_1, s_2 and s_3 are time averages over electric field components resulting in the total intensity (s_0), the intensity difference between p and s polarized light (s_1), $+45^\circ$ and -45° linearly polarized light (s_2), and the right and left polarized part of the light (s_3).

#197203 - $15.00 USD Received 13 Sep 2013; revised 18 Nov 2013; accepted 18 Nov 2013; published 9 Dec 2013

The change of polarization upon interaction with a sample using the Stokes vector is described using the 4×4 element Mueller matrix. For reflection measurements of an isotropic surface the Mueller matrix is

$$\mathbf{M}_{\text{iso}} = \begin{bmatrix} 1 & -\cos 2\Psi & 0 & 0 \\ \cos 2\Psi & 1 & 0 & 0 \\ 0 & 0 & \sin 2\Psi \cos\Delta & \sin 2\Psi \sin\Delta \\ 0 & 0 & -\sin 2\Psi \sin\Delta & \sin 2\Psi \cos\Delta \end{bmatrix}, \tag{3}$$

where Ψ and Δ are the two classical ellipsometric angles found taking the ratio of the Fresnel coefficients $r_{pp}/r_{ss} = \tan\Psi \exp(i\Delta)$, see *e.g.* Azzam and Bashara [27]. In Mueller matrix ellipsometry the Mueller matrix is measured directly, and may, for anisotropic samples, have no elements that are zero. Then the coupling between the *s* and *p* polarized light becomes important, and the corresponding Mueller matrix expressed using the Fresnel reflection coefficients from the Jones matrix (Eq. (1)) becomes [28]

$$\mathbf{M}_{\text{aniso}} = \begin{bmatrix} \frac{1}{2}(|r_{pp}|^2+|r_{sp}|^2+|r_{ps}|^2+|r_{ss}|^2) & \frac{1}{2}(|r_{pp}|^2+|r_{sp}|^2-|r_{ps}|^2-|r_{ss}|^2) & \dots \\ \frac{1}{2}(|r_{pp}|^2-|r_{sp}|^2+|r_{ps}|^2-|r_{ss}|^2) & \frac{1}{2}(|r_{pp}|^2-|r_{sp}|^2-|r_{ps}|^2+|r_{ss}|^2) & \dots \\ \text{Re}(r_{pp}r_{sp}^*+r_{ps}r_{ss}^*) & \text{Re}(r_{pp}r_{sp}^*-r_{sp}r_{ss}^*) & \dots \\ -\text{Im}(r_{pp}r_{sp}^*+r_{ps}r_{ss}^*) & -\text{Im}(r_{pp}r_{sp}^*-r_{ps}r_{ss}^*) & \dots \end{bmatrix}$$
$$\begin{bmatrix} \text{Re}(r_{pp}r_{ps}^*+r_{sp}r_{ss}^*) & \text{Im}(r_{pp}r_{ps}^*+r_{sp}r_{ss}^*) \\ \text{Re}(r_{pp}r_{ps}^*-r_{sp}r_{ss}^*) & \text{Im}(r_{pp}r_{ps}^*-r_{sp}r_{ss}^*) \\ \text{Re}(r_{pp}r_{ss}^*+r_{ps}r_{sp}^*) & \text{Im}(r_{pp}r_{ss}^*-r_{ps}r_{sp}^*) \\ -\text{Im}(r_{pp}r_{ss}^*+r_{ps}r_{sp}^*) & \text{Re}(r_{pp}r_{ss}^*-r_{ps}r_{sp}^*) \end{bmatrix}. \tag{4}$$

When reporting Stokes vectors and Mueller matrices, they are normalized to the first (s_0 and $\mathbf{M}_{11}$) element.

The spectroscopic Mueller matrix can through the appropriate modelling be used to invert for the dispersive optical properties of thin plasmonic layers/plasmonic surfaces. Commonly available effective medium theories, such as Yamaguchi [29, 30], anisotropic Bruggeman [31] and anisotropic Maxwell-Garnett [32], do not well capture the plasmonic response of nanoparticles on a substrate. Furthermore, tabulated reference optical properties of metallic nanoparticles are uncertain. On the other hand, recent rigorous numerical approaches [2, 33, 34] require the particles to be of regular shape and regularly distributed, and in [2] not in direct contact with the substrate. However, the latter approach supplies useful physical insight into the line shape of the dielectric function. An appropriate and practical approach to extract the intrinsic optical response of the nano-plasmonic layer, is to make an anisotropic parametric dispersion model based on oscillators in order to capture the plasmonic, interband and free electron response, in addition to appropriate Euler angles to capture the possibility of a biaxial dielectric tensor with principal axes tilted away from the substrate normal. This model allows to simulate and compare to the large Mueller matrix data set. By trial an error, a reasonable set of starting parameters can be found, and finally fitted to the full data-set. As the nanowires are anisotropic, the dielectric function is a tensor with at most three orthogonal axes with different properties when assuming an orthogonal coordinate system. The inherent tilt and the truncation of the gold nanoparticles on the ripple surface, suggested a *biaxial* tensor with appropriate Euler angles. The anisotropic dispersion model approach is here used to determine the biaxial dielectric tensor and the Euler angles for the gold nanowires deposited on the quartz ripple substrate.

#197203 - $15.00 USD Received 13 Sep 2013; revised 18 Nov 2013; accepted 18 Nov 2013; published 9 Dec 2013

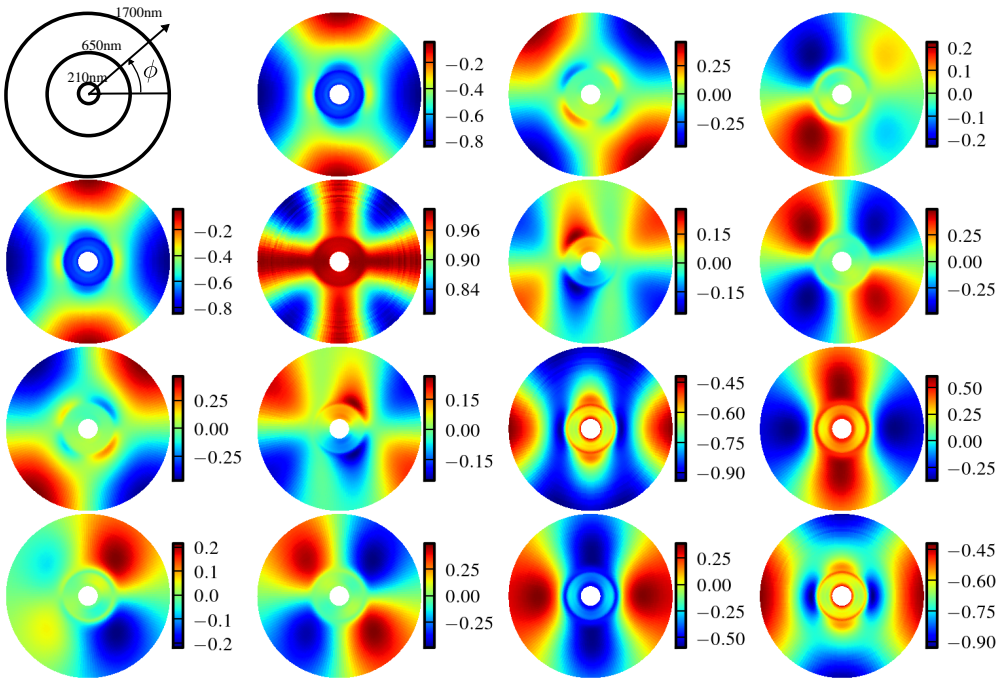

Fig. 3. A polar color map of the experimental spectroscopic Mueller matrix measured at 50° incidence. The radius correspond to the wavelength from 210 nm (5.9 eV) at the inner radius circle to 1700 nm (0.73 eV) at the outer edge. The Mueller matrix is normalized to the m_{11} element. The color bar shows the scale at each element.

4. Results and discussions

Figure 3 shows the fascinating information captured by the full spectroscopic Mueller matrix recorded at 50° incidence for a complete azimuthal rotation of the sample. The Mueller matrix is here presented as a polar color map, where the wavelength is mapped linearly to the radial direction, and the incidence plane orientation is mapped to the polar angle. The color map shows the numerical value of the Mueller matrix element at a particular incidence plane and wavelength, at the given incidence angle. The incidence plane has initially been rotated so that 0° and 90° correspond to the directions where the block off-diagonal elements are at a minimum, a close to pseudo isotropic orientation where the Mueller matrix may be approximated using Eq. (3), i.e. the incidence plane is coinciding with the long and short axis of the nanowires.

In Fig. 4 the Mueller elements m_{12}, m_{33} and m_{34}, *i.e.* the standard ellipsometric parameters N, C and S, respectively, are plotted for these two incidence planes ($\phi = 0°$ and 90°) for the incidence angles $\theta = 50°$, 60° and 70°, as a function of photon energy. All three elements shows large differences between the two incidence planes. In particular, below 3 eV the difference is largest, while for higher energies the data is similar.

The fabrication method employed leads to the formation of gold nanowires which are preferentially aligned along the side of the quartz nano ripples illuminated by the gold atom flux during evaporation, as illustrated in Fig. 2. For the optical model, localized surface plasmon resonances from strictly monodisperse noble metal nanoparticles in a well defined infinite regular

#197203 - $15.00 USD Received 13 Sep 2013; revised 18 Nov 2013; accepted 18 Nov 2013; published 9 Dec 2013

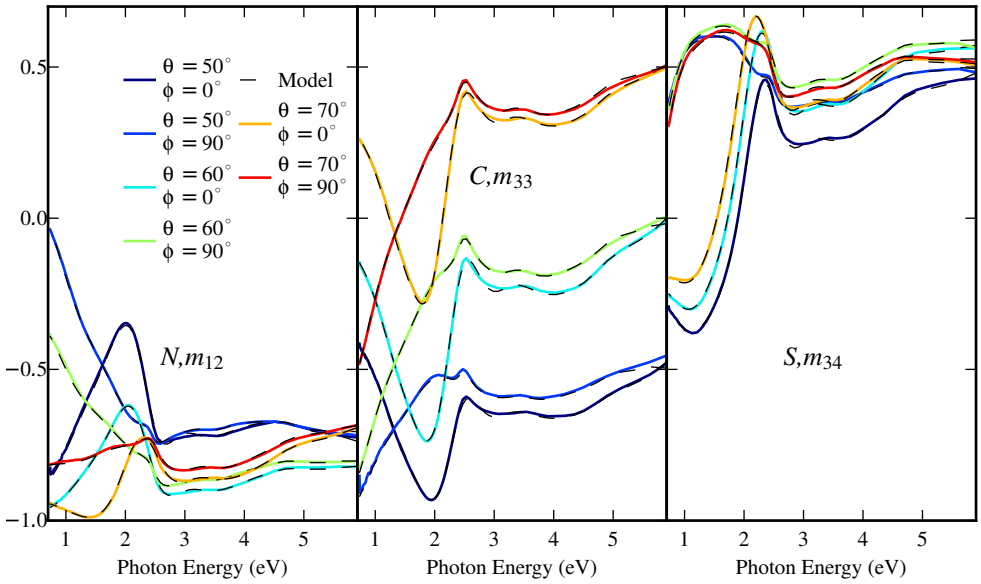

Fig. 4. The spectroscopic Mueller matrix elements m_{12}, m_{33} and m_{34} for the incidence angles 50° and 70° and incidence planes 0° and 90°. The solid colored lines show the experimental data, while the dashed black lines show the simulated data.

array can be modelled by a Lorentzian line shape given by [35]

$$\tilde{\varepsilon}_{\text{Lorentz}}(E) = \frac{A_k}{E_k^2 - E^2 - i\gamma_k E}, \tag{5}$$

where A_k is the amplitude, E_k energy location, γ_k a broadening parameter and E the photon energy. Such a Lorenzian model may be readily understood also in terms of Maxwell-Garnett theory for particles within a host matrix. Normal to the local plane surface which is supporting the gold particles (z-direction), the model also includes a standard Drude dispersion term [35]

$$\tilde{\varepsilon}_{\text{D}}(E) = -\frac{E_p^2}{E^2 + i\gamma_k E}, \tag{6}$$

where E_p is the plasma energy and γ_k is the broadening parameter.

The self-organized formation of the nano ripples recurring to a stochastic process of sputtering may result in small variations of the plasmon resonance energy. This can be represented by a sum of Lorentzians distributed around a center energy E_k. The resulting line shape may for the imaginary part of the dielectric function then more simply be expressed by a Gaussian line shape

$$\varepsilon_{\text{2Gauss}} = A_k \left[\exp\left\{ -\left(\frac{E - E_k}{\gamma_k} \right)^2 \right\} + \exp\left\{ -\left(\frac{E + E_k}{\gamma_k} \right)^2 \right\} \right], \tag{7}$$

where the parameters γ_k is the broadening, A_k the amplitude and E_k the center energy position. Equation (7) is a sum of two Gaussians with positive and negative center energy making it an odd function which is needed for Kramers-Kronig consistency [36]. The real part of the

#197203 - $15.00 USD Received 13 Sep 2013; revised 18 Nov 2013; accepted 18 Nov 2013; published 9 Dec 2013

dielectric function is calculated using Kramers-Kronig relations, and results [36]

$$\varepsilon_{1\text{Gauss}} = A_k \left[\Gamma\left(\frac{E - E_k}{\gamma_k} \right) + \Gamma\left(\frac{E + E_k}{\gamma_k} \right) \right]. \tag{8}$$

Here Γ is a convergence series that produces the Kramers-Kronig consistent line shape.

We let the localized plasmons be described by one or several Gaussians, where each localized plasmon is denoted ε_{Loc}. Several localized plasmons was found necessary to account for a distribution of nano particle sizes, and a distribution of connectivity between the particles. The Drude contribution ε_D is the special case of near bulk gold behaviour such as expected for completely connected nanowires. For simplicity of the model, the interband contribution are accounted for by a single Gaussian (Eq. (7)), denoted ε_{IB}. The dielectric function for the three tensor components $q = x, y, z$ is then proposed described by:

$$\tilde{\varepsilon}^q_{\text{Total}}(E) = \varepsilon^q_\infty + \sum \varepsilon^q_{\text{Loc}} + \varepsilon^q_{\text{IB}} + \varepsilon^q_{\text{D}} \tag{9}$$

A total of 9 oscillators were needed in order to have an acceptable mean square error between the simulated and measured data. Three oscillators for each direction. The complex inverse problem was found to be most easily solved using an iterative process. First, the common ellipsometric parameters (*N*, *C* and *S*) were used to determine an approximate solution to the biaxial effective dielectric tensor by assuming that the principal axes of the tensor were in the sample plane. All incidence planes and the different incidence angles were used in order to increase the sensitivity to the effective properties normal to the surface (z-direction). The (*N*, *C* and *S*) parameters were also found to be most sensitive to the effective layer thickness, such that the first analysis supplied an estimate of the effective film thickness in addition to a first estimate to the dielectric tensor.

Upon rotation of the incidence plane, it is observed from the polar plots in Fig. 3 that the block-diagonal Mueller elements have a 180° symmetry. The off block-diagonal elements, which are probing the cross polarization *i.e.* the anisotropy (cf. Eq. (4)) show a more complex behaviour. It is particularly observed that they are oscillating with a different amplitude for the maxima and mimima. Further, for $\phi = 0^\circ$ (incidence plane normal to the nanowires) the Mueller matrix is pseudo-isotropic (i.e. a diagonal Jones matrix).

The metallic nano particles on a substrate indicate that the dielectric tensor has principal axes aligned with, and perpendicular to the local surface normal. The local slope (θ in Fig. 2) is approximated to be the Euler rotation angle for the dielectric tensor. The $z-$axis of the tensor is then no longer orthogonal to the global sample plane and does also have a component in the $y-$direction, in principle one could expect that the plasmonic resonance may also be weakly observed in this part of the dielectric tensor. The off-diagonal elements were therefore used to fit the tilt angle θ by applying an Euler rotation of the dielectric tensor. This process was repeated until convergence.

The tilt angle converged to 12.8° and the effective thickness of the nanoparticle film amounts to 28 nm. The parameters were found to have an accuracy within ± 4 nm and $\pm 2^\circ$. The parameters of the dielectric tensor is summarized in Table 1, while Figure 5 shows the real and imaginary part of the dielectric functions for the three principal axes, where we have used the fitted dispersion model parameters in Table 1.

The mean square error for the final model was MSE = 9.7 [38] when evaluating 32 free parameters, using 50 incidence planes, 6 incidence angles and 1067 wavelengths. In the calculation of the MSE the uncertainty in each data point in the Mueller matrix was estimated to 0.001.

The most striking feature in Fig. 5 is the localized plasmonic resonance peak at 1.58 eV for

#197203 - $15.00 USD Received 13 Sep 2013; revised 18 Nov 2013; accepted 18 Nov 2013; published 9 Dec 2013

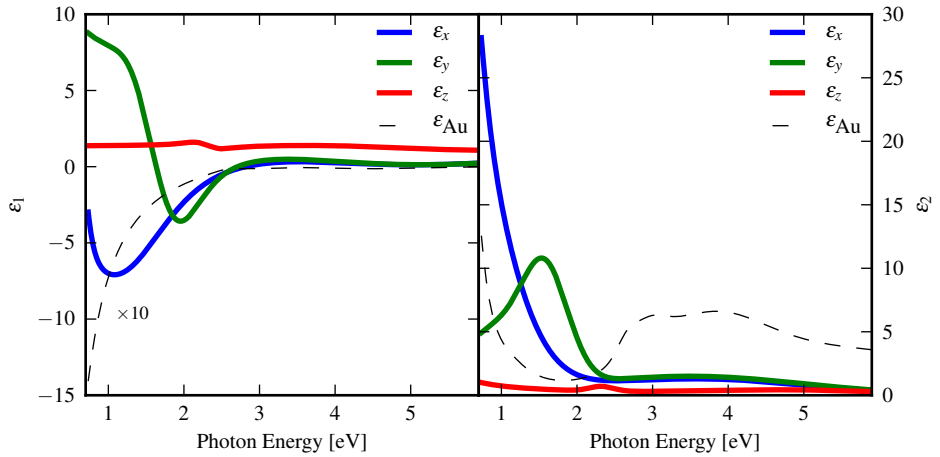

Fig. 5. The complex dielectric tensor parametrized using Eq. (9) and Table 1. The dielectric function of Au [37] is shown for comparison.

Table 1. The parametrization of the dielectric tensor of the film. The amplitudes, broadening and energy corresponds to the parameters of a Lorentzian, Drude and Gaussian line shapes in Eq. (5), Eq. (6) and Eq. (7). The blank fields indicate that the oscillator was not included for the corresponding axis.

	x			y			z			
	A_k	γ_k	E_k	A_k	γ_k	E_k	A_k	E_p	γ_k	E_k
$\varepsilon_{\mathrm{Loc1_{Gauss}}}$	53.43	0.92	0.13	8.67	0.43	1.58	0.48	–	0.20	2.33
$\varepsilon_{\mathrm{Loc2_{Gauss}}}$	–	–	–	4.30	0.68	0.87	–	–	–	–
$\varepsilon_{\mathrm{Loc2_{Lorentz}}}$	22.69	0.47	0.60	–	–	–	–	–	–	–
$\varepsilon_{\mathrm{IB_{Gauss}}}$	1.39	2.22	3.75	1.66	2.31	3.57	0.42	–	1.69	4.83
ε_{D}	–	–	–	–	–	–	–	2.47	6.58	–
ε_∞		1.41			1.41			1.43		

the ε_y component (normal to the wires, but in the sample plane), although it also appears to contain an additional localized plasmonic feature around 0.9 eV. The ε_x component appears to contain strong contributions from two localized plasmons located in the IR region of the spectrum. The exact locations of these plasmons are uncertain, and may be further revealed in upcoming work using IR Mueller matrix ellipsometry. As previously mentioned, it is speculated that several such localized plasmons may be the result of incomplete connectivity within the chains of particles making up the ”nanowires” along the x-axis. A completely connected chain should thus be represented by the Drude model, while the reduced chain lengths may result in the IR localized plasmons. For comparison a typical dielectric function for Au is included in Fig. 5. The interband transitions in the plasmonic film are strongly attenuated compared to Au, and the plasmon resonances in ε_x, ε_y and ε_z makes ε_1 increasing in the infrared.

An interband contribution with center energy 3.75 eV and 3.57 eV was found for both the ε_x and ε_y components. The ε_z component was found to be dominated by a weak Drude component in the near infrared and some weak interband contribution with center energy 4.83 eV. Another weak localized plasmon contribution at 2.33 eV appeared in ε_z. The blue shift for the out of plane resonance follows the results of polarizability calculations for silver hemispherical islands on MgO substrate by Lazzari and Simonsen [33]. The ε_z component also has a Drude

#197203 - $15.00 USD Received 13 Sep 2013; revised 18 Nov 2013; accepted 18 Nov 2013; published 9 Dec 2013

component, which was also found for silver hemispherical nanowires supported on silicon substrate in [10], while the effective film appears much less dense compared to bulk Au properties. The blue shifted out of plane resonance predicted by Lazzari and Simonsen was, however, not reported by Oates *et al.* [10]. The effective thickness of the layer is probably much larger than the truncated particle thickness on the "hills" of the ripple along the z-axis, i.e. the local surface normal.

In Fig. 6 the measured spectroscopic Mueller matrix at 50° incidence for the incidence planes 0°, 45°, 135°, 180°, 225° and 270° is plotted together with the simulated data using the fitted parametric model. The simulated data is also plotted as dashed lines for different incidence angles in Fig. 4. The figure of merit was calculated using the root mean square error of the entire data set, where the weighting on all Mueller matrix elements and measured wavelengths in nm are the same.

In order to verify the optical model, a direct analysis of the slope distribution of the AFM image in Fig. 1(a) was performed. Fig. 7 shows a histogram of the slope in the image. It is found that the most dominant inclination is 12°-13°, which much verify the tilt angle found by Mueller matrix ellipsometry.

The polarizing properties of the sample was investigated by spectroscopic transmission Mueller matrix measurements. Figure 8 shows the measured data at normal incidence as a solid curve and the simulated data using the model from above, where only the relative orientation of the sample was refitted. The simulations reproduce all features of the measurement,

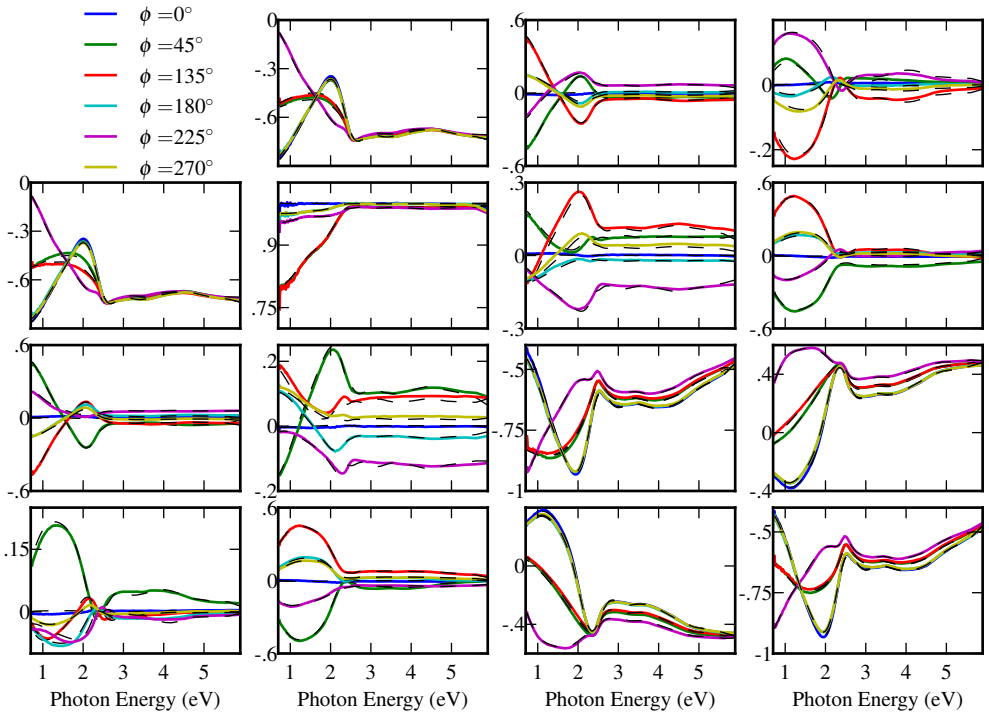

Fig. 6. The spectroscopic Mueller matrix at 50° incidence for six incidence planes (0°, 45°, 135°, 180°, 225° and 270°). The solid colored curves show experimental data, while the dashed black curves show the simulated data.

#197203 - $15.00 USD Received 13 Sep 2013; revised 18 Nov 2013; accepted 18 Nov 2013; published 9 Dec 2013

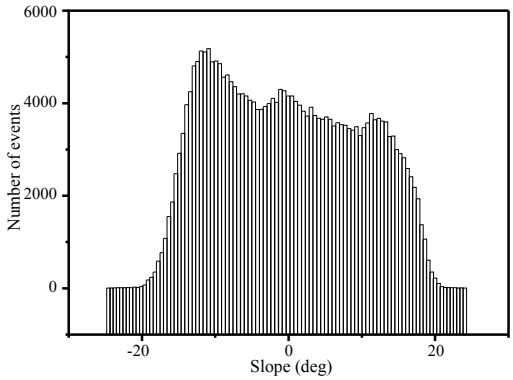

Fig. 7. Histogram showing the distribution of slope for the AFM image in Fig. 1(a).

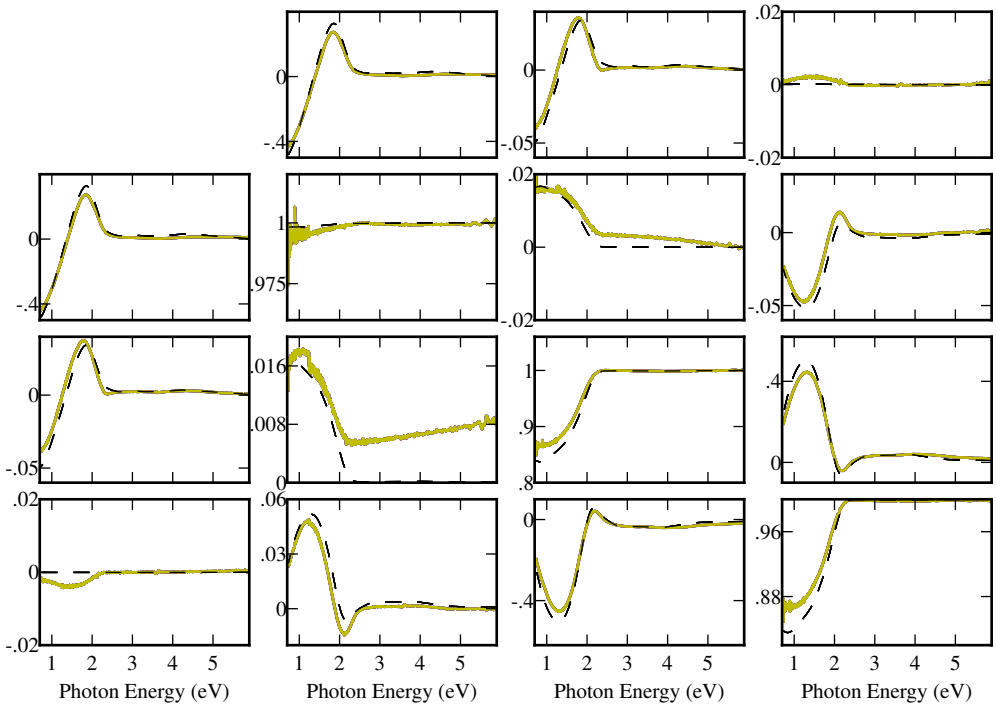

Fig. 8. Spectroscopic Mueller matrix measurement in transmission. The solid line indicates the measurement, while the dashed line is the simulated data using the model in Table 1

#197203 - $15.00 USD Received 13 Sep 2013; revised 18 Nov 2013; accepted 18 Nov 2013; published 9 Dec 2013

except a very small Gaussian like "bump" (amplitude 0.002) in the $m_{14/41}$ elements indicating an induced circular dichroism. The Mueller matrix is largely block-diagonal, meaning that the optical axis of the sample coincide with the axes of the instrument, only small deviations of a few per cent origin from sample orientation misalignment of approximately 3°.

The linearly polarizing properties are directly observed in the $m_{12/21}$ elements, and through the model, we can now observe that the main features are related to the plasmon resonances in ε_y and ε_x.

For the y direction the transmission measurements show a peak at 1.84 eV that is the maximum in the extinction coefficient $\kappa = \varepsilon_2/2n$, where n is the real part of the refractive index $n^2 = \frac{1}{2}\varepsilon_1 + \frac{1}{2}\sqrt{\varepsilon_1^2 + \varepsilon_2^2}$. In the infrared, the $m_{12/21}$ elements are negative due to the resonance in the ε_x. This anisotropy is of inverse polarizing character [39, 40], where the polarization shifts spectrally.

The features in the lower right 2×2 matrix comes from the spectral birefringence ($\Delta n = n_x - n_y$). A polar decomposition [41] of the Mueller matrix supplies the magnitude and orientation of the retarding and diattenuating (polarizing) properties. Figure 9(a) shows the linear retardance (δ) and the linear diattenuation, the corresponding orientation of the slow axis (θ_δ) and the orientation of the transmission axis (θ_D) are plotted in Fig. 9(b). By analysing Fig. 9 in detail, it is observed that the sample works as a polarizer with transmission axis along the y-axis in the infrared range. At approximately 1.4 eV the sample is a pure retarder (minimum diattenuation and maximum retardance), while at approximately 2 eV the sample is a polarizer with transmission axis along the x-direction. These properties can in principle be shifted spectrally by varying the period of the ripple structure and consequently the distance between the nanowires [2]. It is also expected that the density of the particles forming the nanowires would change the resonance frequency, from a pure Au response for perfect wires, to a response dominated by localized surface plasmon resonances for separated particles.

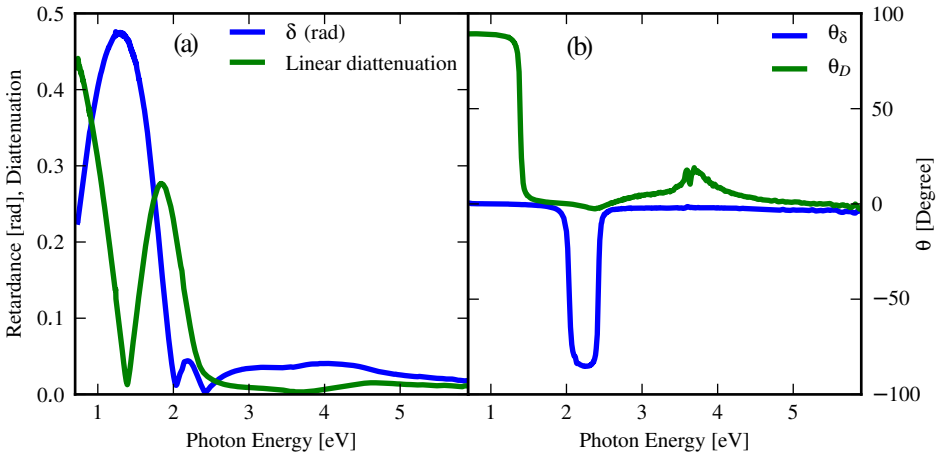

Fig. 9. Figure (a) shows the retardance (δ) and the diattenuation of the transmission Mueller matrix, while Fig. (b) shows the orientation of the corresponding slow axis and transmission axis.

5. Conclusion

The localized plasmonic optical properties of in plane gold nanowire array deposited at grazing incidence on a nano-ripple quartz substrate has been determined by variable angle spectroscopic

#197203 - $15.00 USD Received 13 Sep 2013; revised 18 Nov 2013; accepted 18 Nov 2013; published 9 Dec 2013

Mueller matrix ellipsometry (MME) with complete azimuthal rotation of the sample. The sensitivity to the anisotropy is strong in all Mueller elements, including the elements measured in standard ellipsometry. The off block-diagonal elements show a lower symmetry, suggesting that the shadowing effects during deposition leaves the nano-wires tilted with respect to the surface normal. The dielectric tensor axes are proposed tilted by the same angle, as was found non-destructively by MME. The three components of the dielectric tensor were determined through parametric dispersion models for each component. The extracted dielectric functions complete the understanding of the observed wire-grid and inverse polarizing properties. The parametric dispersion models extracted from the effective thin surface layer composed of aligned gold nanoparticles on the nano-ripple glass surface, is expected to be a useful model starting point for many similar nano-plasmonic systems. Finally, a systematic approach was proposed to attack the complex modelling issue with such a large MME data-set.

Acknowledgments

L.M.S.A acknowledges financial support from "The Norwegian Research Center for Solar Cell Technology" (project num. 193829).
This work has been partly supported by MAE under program Italia-Polonia, and by MSE in the framework of the Operating Agreement with ENEA for research on the Electric System.

#197203 - $15.00 USD Received 13 Sep 2013; revised 18 Nov 2013; accepted 18 Nov 2013; published 9 Dec 2013